9266–9278 *Nucleic Acids Research, 2016, Vol. 44, No. 19* *Published online 25 July 2016*
doi: 10.1093/nar/gkw663

OGT restrains the expansion of DNA damage signaling

Qiang Chen and Xiaochun Yu*

Department of Cancer Genetics and Epigenetics, Beckman Research Institute, City of Hope, 1500 E. Duarte Road, Duarte, CA 91010, USA

Received February 10, 2016; Revised July 5, 2016; Accepted July 13, 2016

ABSTRACT

O-linked N-acetylglucosamine linkage (O-GlcNAcylation) to serine or threonine residues regulates numerous biological processes; however, its role in DNA damage response remains elusive. Here, we found that O-GlcNAcylation is induced by DNA damage response. O-GlcNAc transferase (OGT), the solo enzyme for O-GlcNAcylation, relocates to the sites of DNA damage and induces the O-GlcNAcylation of histone H2AX and mediator of DNA damage checkpoint 1 (MDC1). The O-GlcNAcylation negatively regulates DNA double-strand break-induced phosphorylation of H2AX and MDC1 by restraining the expansion of these phosphorylation events from the sites of DNA damage. Therefore, our study reveals the molecular mechanism and biological function of OGT-dependent O-GlcNAcylation in response to DNA damage.

INTRODUCTION

In response to DNA damage, multiple DNA damage repair factors relocate to the sites of DNA damage for the activation of DNA damage repair and cell cycle checkpoints (1–5). The dynamic relocation of DNA repair factors is mediated by DNA damage-induced post-translational modifications (PTMs) on histones and their binding partners at, or adjacent to, the sites of DNA damage (6–8). One of the key DNA damage-induced epigenetic modifications is the phosphorylation of histone H2AX (aka γH2AX) (9,10). This unique DNA damage-induced phosphorylation event is catalyzed by a group of phosphatidylinositide 3 (PI-3)-like kinases, including ataxia telangiectasia mutated (ATM) (11–14), ATM and Rad3 related (ATR) (15), and DNA-dependent protein kinase (DNA-PK) (16–18). γH2AX creates a phospho-epitope that is engaged by the mediator of DNA damage checkpoint protein 1 (MDC1) BRCA1 carboxy-terminal (BRCT) domain (19,20). MDC1 is subsequently phosphorylated by ATM, which creates binding sites to recruit other DNA damage response proteins (21,22). Although these phosphorylation events can gradually expand to a mega-base region from the site of DNA damage, they are still restrained to a relatively small compartment compared to the size of whole genome (10), and underlying molecular mechanism is unclear. Furthermore, these DNA damage-induced phosphorylation events can last for more than 24 h (23), which is critical for DNA damage response such as cell cycle checkpoint activation. Therefore, it is intriguing to understand the molecular mechanism by which DNA damage-induced signaling is limited.

The PI-3-like kinases, such as ATM, mainly phosphorylate Serine (Ser) or Threonine (Thr) residues on their substrates. Interestingly, Ser or Thr residues can also be modified by O-GlcNAcylation, a unique PTM catalyzed by the O-GlcNAc transferase (OGT) (24–26). OGT is an evolutionarily conserved polypeptide with 1046 residues, including 13.5 N-terminal tetratricopeptide repeats (TPRs) and a C-terminal catalytic domain (27). With UDP-GlcNAc as the donor, OGT removes UDP and covalently links the N-acetylglucosamine (GlcNAc residue) to the hydroxyl side chain of Ser or Thr, resulting a single O-linked GlcNAc (O-GlcNAc) on the substrates (27). The same Ser and Thr residues, on substrates such as c-Myc proto-oncogene and RNA polymerase II, can be modified by both O-GlcNAcylation and phosphorylation (28–30). Therefore, it has been proposed that O-GlcNAcylation and phosphorylation may compete for the same amino acids on key cellular proteins (31). In support of a complex relationship between O-GlcNAcylation and phosphorylation (28–30,32–35), elevating O-GlcNAc levels decreases phosphorylation (36) and *vice versa* (34). Thus, it is likely that O-GlcNacylation antagonizes phosphorylation in many biological events and may regulate γH2AX expansion after DNA damage.

Here, we tested the role of O-GlcNacylation in DNA damage-induced signaling. We found that OGT relocates to the sites of DNA damage and catalyzes O-GlcNAcylation of H2AX and MDC1. These O-GlcNAcylation events suppress the expansion of DNA damage-induced phosphorylation events on the chromatin.

MATERIALS AND METHODS

Plasmids, antibodies, siRNAs and chemical reagents

The full-length cDNA of human OGT was cloned into the pEGFP-C1 vector. Internal deletion mutants and the enzyme-dead mutant (G598S) of OGT were generated us-

*To whom correspondence should be addressed. Tel: +1 626 218 5724; Fax: +1 626 218 0403; Email: xyu@coh.org

ing the QuickChange site-directed mutagenesis kit (Stratagene). Deletion mutants of OGT were constructed as described previously (37).

Antibodies used in this study include the following: anti-OGT antibody (Novaus), anti-γH2AX (Upstate Biotechnology, monoclonal and polyclonal), anti-O-GlcNAc (RL2 monoclonal [Abcam] and CTD110.6 monoclonal [Covance]), anti-FLAG (Sigma), anti-Myc (Sigma), anti-Actin (Sigma), anti-Mdc1 (Sigma), anti-PAR (Genetex, monoclonal), anti-Ku80 (Cell Signaling Technology), anti-Chk1 (Cell Signaling Technology), anti-phospho-Chk1 (Ser345,Cell Signaling Technology) and anti-phospho-SQTQ (Cell Signaling Technology). siRNA sequences were generated to target human OGT (5′-GCACATAGCAATCTGGCTTCC-3′ or 5′-CCAAACTTTCTGGATGCTTAT-3′).

The OGT inhibitor (ST045849) was purchased from TimTec and the O-GlcNAcase (OGA) inhibitor (PUGNAc) was purchased from Toronto Research Chemicals. The ATM inhibitor KU-55933 was purchased from Calbiochem. For cell treatment, a final concentration of 2 μM KU-55933 was added to the cell medium at the indicated timepoints.

Recombinant proteins and *in vitro* assays

Recombinant His-tagged H2AX proteins were purified from *Escherichia coli* cells. Recombinant streptavidin binding peptide (SBP)-tagged OGT protein was purified from Sf9 insect cells. For the *in vitro* O-GlcNAcylation assay, recombinant SBP–OGT protein (0.5 μg) was incubated with 2 μg substrates and 0.5 mM (0.5 uCi) UDP-[^{3}H]GlcNAc (from American Radiolabeled Chemicals) in 25 μl reaction buffer (50 mM Tris–HCl, pH 7.5, 12.5 mM MgCl2 and 1 mM dithiothreitol [DTT]) for 1 h at 37°C. The reaction was stopped by 10 mM ethylenediaminetetraacetic acid (EDTA). For the histone glycosylation analyses, the reaction was resolved with sodium dodecyl sulphate-polyacrylamide gel electrophoresis (SDS-PAGE), and then subjected to autoradiography after incubation with EN3HANCE (from PerkinElmer). For the ATM-dependent *in vitro* kinase assays, FLAG-tagged ATM was transiently transfected into 293T cells and immunoprecipitated using anti-FLAG M2-agarose (Sigma). The immunoprecipitates were extensively washed and then incubated with substrates in the kinase buffer (25 mM HEPES [pH 7.4], 50 mM NaCl, 10 mM MnCl2, 10 mM MgCl2, 1 mM DTT, 5 μM ATP) at 30°C for 30 min. The phosphorylated proteins were separated by SDS-PAGE and western blotted with an anti-γH2AX antibody.

Cell lysis, immunoprecipitation (IP) and western blotting

The cells were harvested at the indicated time points after 10 Gy of ionizing radiation (IR) treatment and washed twice with phosphate buffered saline (PBS). The cell pellets were subsequently resuspended in NETN lysis buffer (20 mM Tris–HCl, pH 8.0, 100 mM NaCl, 1 mM EDTA and 0.5% NP-40) and incubated on ice for 10 min. Thereafter, the insoluble fractions were digested by Benzonase to extract the chromatin fraction, then subjected to electrophoresis or immunoprecipitation followed by western blot analysis.

Laser micro-irradiation, immunofluorescence (IF) staining and microscope image acquisition

To generate DNA damage in cells, we adopted laser micro-irradiation method, which has the privileges on the study of the kinetics of proteins or protein-modifications recruitment and dynamics after DNA damage.

For laser micro-irradiation, the cells were grown on 35 mm glass bottom dishes (MatTek Corporation). Laser micro-irradiation was performed on an OLYMPUS IX71 inverted fluorescence microscope with a Micropoint Laser Illumination and Ablation System (Photonic Instruments). High energy UV laser was generated from the Micropoint Laser Illumination and Ablation System and focused into the cell nucleus through the light path of the microscope to generate DNA breaks. By moving the stage of the microscope, the laser drew a line of DNA damage inside of nucleus without rapturing the nuclear membrane or cell membrane. The damaged DNA could be visualized by immunostaining with anti-γH2AX antibody as γH2AX is a surrogate maker of DNA lesion. The laser output was set to 40%, which can reproducibly produce a focused γH2AX stripe. For time-lapse microscopy analysis, the cells were first transfected with the corresponding plasmids. Then, the green fluorescent protein (GFP)-positive cells were subjected to micro-irradiation. The micro-irradiated strips of GFP-positive cells were evaluated at the indicated time points and then analyzed with the Image J software program. For time course analysis of laser micro-irradiation, the samples were subjected to continuous micro-irradiation along certain paths, within the indicated time interval. Then, the samples were subjected to immunofluorescence (IF) staining. For IF staining with the anti-OGT or anti-O-GlcNAc antibodies, the cells were permeabilized with 0.5% Triton X-100 for 5 min at room temperature. The samples were then incubated with the primary antibodies for 1 h. The samples were washed three times, incubated with the secondary antibodies for 30 min at room temperature and visualized with an OLYMPUS IX71 inverted fluorescence microscope. All of the images were acquired with the cellSens standard (Version 1.3) software. Identical contrast and brightness adjustments were used on images for all experiments. The width of laser strips at indicated time points was analyzed by Image J. Normalized fluorescent curves from 10 cells from three independent experiments were averaged for each indicated sample. Error bars represent the standard deviation. For the 3D surface plot, the images were analyzed using Image J.

Alkaline comet assay

Single-cell gel electrophoretic comet assays were performed under alkaline conditions. Briefly, 24 h after electroporation of the indicated plasmids, or transfection with the indicated siRNA, HeLa cells were irradiated with or without 5 Gy of IR and allowed to recover in normal culture medium for the indicated time at 37°C. The cells were collected and rinsed twice with ice-cold PBS; 2×10^4/ml cells were combined with 1% LMAgarose at 40°C at a ratio of 1:3 (v/v) and immediately pipetted onto slides. For cellular lysis, the slides were immersed in the alkaline lysis solution (1.2 M NaCl, 100 mM EDTA, 0.1% SDS and 0.26 M NaOH, pH > 13)

overnight at 4°C. Then, the slides were subjected to electrophoresis at 15 V for 25 min (0.6 V/cm) and stained in 10 μg/ml propidium iodide for 20 min. All images were taken with a fluorescence microscope and analyzed by the Comet Assay IV software program.

RESULTS

γH2AX signals are expanded at the sites of DNA damage

Phosphorylation of H2AX at Ser 139 (γH2AX) is one of the early and key processes in DNA damage response; it stabilizes numerous DNA damage response factors at the sites of DNA double-strand breaks (DSBs) (3). It has been shown that γH2AX is present on the chromatin that flanks DNA damage sites (9,10,13,19). To examine the kinetics of γH2AX, we measured the peak intensity of γH2AX to monitor the peak level of γH2AX at the sites of DNA damage. We also measured the width of the laser strip [full width at half maximum (FWHM)] to examine the expansion of γH2AX. Moreover, we calculated the overall intensity of γH2AX (triangular area with γH2AX signal, as shown in Figure 1A) in response to laser micro-irradiation (Figure 1A). One minute after the DNA damage, γH2AX became visible at the sites of DNA damage (Figure 1B). Within 10 min after the DNA damage, the γH2AX signal was not only remarkably enhanced at the sites of DNA damage, but it had also expanded to the adjacent area (Figure 1B). However, the γH2AX signal, including the peak level, width of the strip and overall intensity, reached a relatively steady state after 10 min of DNA damage, suggesting that other DNA damage response pathways may be activated to limit the expansion of γH2AX in the regions flanking DNA lesions.

O-GlcNAc is induced at the sites of DNA damage

Following DNA damage, the phosphorylation of H2AX is catalyzed by a group of PI-3-like kinases, including ATM, ATR and DNA-PK. Although OGT-dependent O-GlcNAcylation negatively regulates kinase-induced phosphorylation, direct evidence that DNA damage actively induces O-GlcNAcylation has not been reported. To study if O-GlcNAcylation is a DNA damage-induced event, we treated HeLa cells with IR or other DNA-damaging agents. The chromatin fractions of cell lysates were dot-blotted using an anti-O-GlcNAc antibody (CTD110.6) (Figure 2A). We found that the O-GlcNAcylation level was significantly increased after DNA damage. The results were further confirmed using the second anti-O-GlcNAc antibody (Rl2) (Supplementary Figure S1A).

To study the localization of DNA damage-induced O-GlcNAcylation, HeLa cells were subjected to laser micro-irradiation and examined with IF staining using anti-O-GlcNAc antibodies, as well as an anti-γH2AX antibody (Figure 2B). Like γH2AX, O-GlcNAc is clearly enriched at the sites of DNA damage. After blocking the antigen epitopes with excessive GlcNAc, we could not detect DNA damage-induced O-GlcNAcylation, further confirming the specificity of the anti- O-GlcNAc antibodies. Of note, we found that the enrichment of O-GlcNAc at the sites of DNA damage was slower than that of γH2AX (Figure 2C). Taken together, our study suggests that O-GlcNAcylation is a DNA damage-induced PTM.

O-GlcNAcylation suppresses the expansion of γH2AX at the sites of DNA damage

Because O-GlcNAcylation antagonizes phosphorylation, we asked if O-GlcNAcylation negatively regulates H2AX phosphorylation in response to DNA damage. Because O-GlcNAcylation is mediated by OGT, we knocked down OGT using siRNA (Supplementary Figure S1B). OGT depletion not only suppressed the DNA damage-induced O-GlcNAcylation (Supplementary Figure S1C) but also increased the level of γH2AX (Figure 3A). To observe the expansion of γH2AX, we measured the kinetics of the peak level, width and overall intensity of the γH2AX signal in response to laser micro-irradiation in the OGT knockdown cells. We found that the peak level of γH2AX intensity was only slightly increased; however, the width of the laser strip and overall γH2AX signal were significantly increased (Figure 3B).

Moreover, the expansion of γH2AX continued for more than 20 min in response to DNA damage. To carefully observe the signal expansion of γH2AX, we also performed 3D surface plotting of γH2AX 20 min after laser micro-irradiation and found that the laser strip width and overall γH2AX signal were significantly increased, with only a slight increase in the γH2AX peak intensity (Figure 3C and Supplementary Figure S2). To confirm the results, we reconstituted the cells with siRNA-resistant wild-type OGT or the enzyme-dead mutant (OGT-ED). Only the wild-type OGT, but not the ED mutant, could limit the expansion of γH2AX (Figure 3D). Knockdown of OGT, using an siRNA that targets an alternative sequence, produced similar results (Supplementary Figure S3F). In addition, we treated the cells with the OGT inhibitor ST045849. In the presence of ST045849, a similar expansion of γH2AX was observed as that in the OGT-deficient cells (Supplementary Figure S3A and B). Taken together, these results demonstrate that OGT inhibits the expansion of γH2AX in response to DNA damage.

OGT is recruited to the sites of DNA damage

To study the molecular mechanism by which OGT suppresses the expansion of γH2AX, we first examined the localization of OGT in response to DNA damage. Using live cell imaging, we found that OGT was recruited to the sites of DNA damage (Figure 4A). We further confirmed the results by detecting the recruitment of endogenous OGT with an anti-OGT antibody (Supplementary Figure S4A). Again the kinetics of OGT recruitment were much slower than the enrichment of γH2AX, but similar to the enrichment of O-GlcNAc (Figure 4B).

Next, we asked how OGT is recruited to the sites of DNA damage. Because poly(ADP-ribosyl)ation plays a key role in the early establishment of the DNA damage response machinery (38), we asked if poly(ADP-ribosyl)ation is required for OGT recruitment. However, OGT recruitment was unchanged in Parp1 −/− MEFs (Parp1: Poly(ADP-ribose) polymerase-1, MEF: Mouse Embryonic Fibrob-

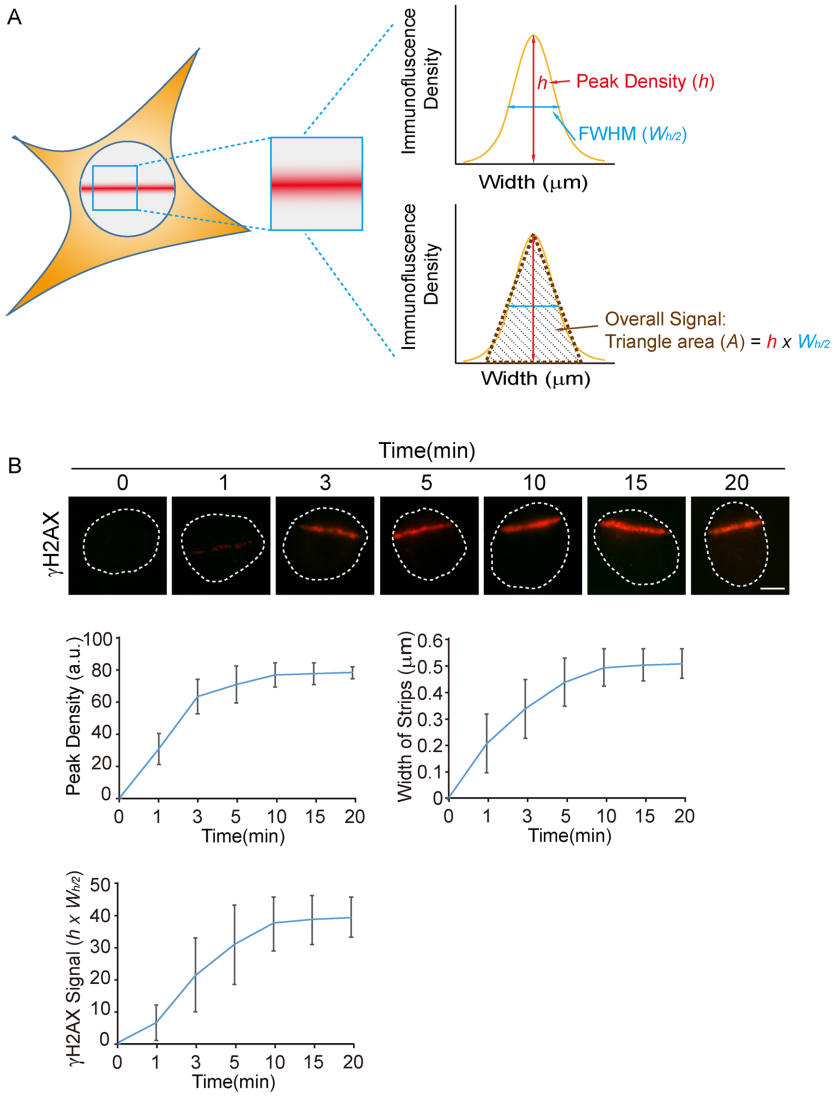

Figure 1. γH2AX signal is quickly expanded at the sites of DNA damage. (**A**) Diagram showing the analyses of the DNA damage signal at the laser micro-irradiation strip. The immunofluorescence (IF) images were analyzed with the Image J software program. The peak IF density (h) refers to the mean peak value across the laser scissor strip. The full width at half maximum (FWHM) ($W_{h/2}$), shown with blue arrows, represents the width of the laser scissor strips. To present the overall signal, the triangular area shown in the right lower panel is calculated using the following formula: triangle area (A) = $h \times W_{h/2}$. (**B**) Kinetics of γH2AX signals in response to laser micro-irradiation (upper panel). The peak IF density, half-peak width and overall signal of γH2AX were plotted against time (lower panel). Scale bar: 5 μm. a.u.: arbitrary units.

last) and in response to PARP inhibitor treatment (Supplementary Figure S4B and C). In addition to poly(ADP-ribosyl)ation, γH2AX is required for the slow accumulation of multiple DNA damage response factors. Next, we examined if H2AX facilitated OGT recruitment in response to laser micro-irradiation. Interestingly, OGT could not be recruited to the sites of DNA damage in H2AX −/− MEFs (Figure 4C); the enrichment of O-GlcNAc also did not occur in H2AX −/− MEFs (Supplementary Figure S4D). As a control, H2AX did not affect the recruitment of the Ku70/80 heterodimer to the sites of DNA damage (Figure 4C). The results suggest that H2AX mediates DNA damage-induced O-GlcNAcylation. We also examined the role of the downstream functional partners of H2AX, but found that OGT recruitment was not affected in MDC1 −/−, RNF8 −/−, 53BP1 −/−, RAP80 −/− MEFs and BRCA1-deficient HCC1937 cells (Figure 4D).

Next, we constructed an OGT deletion mutant that only contains the N-terminal TPR domain (1–510 aa.). We found that the OGT TPR domain could accumulate on the sites of DNA damage (Figure 4E). Furthermore, we constructed six deletion mutants that dissected the function of TPRs on OGT enrichment at DNA damage sites. Interestingly, we found that amino acids 462–510 of OGT, which link the N-terminal TPR and C-terminal catalytic domains, is the key motif for OGT recruitment at the sites of DNA damage (Figure 4E). Next, we expressed the deletion mutant (OGT-D6), which lacks amino acids 462–510, in OGT knockdown cells. In contrast to wild-type OGT, this deletion mutant could not rescue the O-GlcNAcylation at DNA

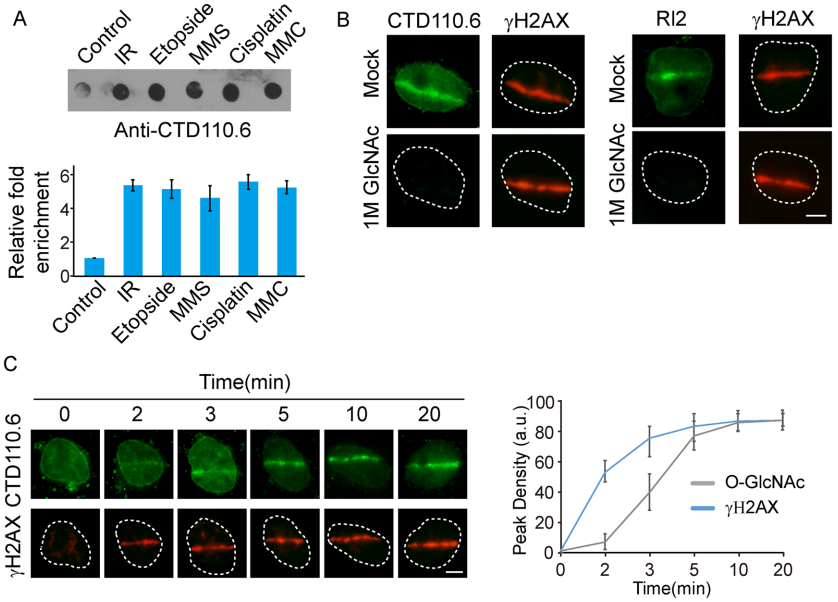

Figure 2. O-GlcNAcylation is enriched at the sites of DNA damage. (**A**) DNA damage induces O-GlcNAcylation. HeLa cells were exposed to multiple DNA damaging agents. The chromatin fractions were dot-blotted with an anti-O-GlcNAc antibody (CTD110.6). The relative intensity of the dots is shown (lower panel). These data represent the mean of duplicate experiments. (**B**) O-GlcNAcylation is enriched at the sites of DNA damage. HeLa cells were subjected to laser micro-irradiation. γH2AX and O-GlcNAcylation (left panel: CTD110.6 and right panel: RI2) were examined by IF. For antibody specificity analysis, 1 M GlcNAc was added to block the epitope. (**C**) The kinetics of O-GlcNAcylation enrichment at the site of DNA damage. HeLa cells were subjected to laser micro-irradiation. At the indicated time points, γH2AX and O-GlcNAcylation (CTD110.6) were examined. The peak fluorescence density of O-GlcNAcylation and γH2AX at the laser strips was quantified at indicated time points by Image J. Scale bar: 5 μm. a.u.: arbitrary units.

damage lesions (Supplementary Figure S1C) and the expansion of γH2AX (Supplementary Figure S3C and D). It has been shown that the TPR domain and the catalytic domain function as a unit to catalyze substrate O-GlcNAcylation. Under normal conditions, the TPR domain associates with the catalytic domains and covers the catalytic site (27). Once OGT encounters its substrate, the TPR domain undergoes massive conformational changes, which expose the catalytic site for substrate O-GlcNAcylation (27). Thus, it is likely that OGT recruitment, substrate recognition and O-GlcNAcylation are tightly associated together.

OGT glycosylates H2AX and MDC1 in response to DNA damage

Because H2AX mediates OGT recruitment, we asked if OGT directly glycosylates H2AX. We treated HeLa cells with IR and the OGA inhibitor PUGNAc to induce DNA damage and suppress the degradation of O-GlcNAcylation. H2AX was immunoprecipitated by an anti-H2AX antibody and the precipitates were O-GlcNAcylated (Figure 5A). To validate the results, we also examined H2AX +/+ and −/− MEFs, and found that H2AX was O-GlcNAcylated in H2AX +/+ MEFs in response to DNA damage (Supplementary Figure S5). siRNA-mediated depletion of OGT remarkably suppressed the O-GlcNAcylation of H2AX (Figure 5A). Similarly, treatment with the OGT inhibitor ST045849 also suppressed DNA damage-induced H2AX O-GlcNAcylation (Figure 5B). Collectively, these results demonstrate that OGT mediates the O-GlcNAcylation of H2AX in response to DNA damage.

Next, we examined the major O-GlcNAcylation sites in H2AX. Large scale mass spectrometry analyses suggest that H2AX can be O-GlcNAcylated at Thr101 (39). We mutated Thr101 to Ala (T101A). However, following DNA damage, the T101A mutant was still O-GlcNAcylated, suggesting that other site(s) on H2AX could be O-GlcNAcylated in response to DNA damage (Figure 5C). Because O-GlcNAcylation negatively regulates H2AX phosphorylation and the major phosphorylation site on H2AX is Ser139, we mutated Ser139 of H2AX into Ala (S139A). Interestingly, the S139A mutation abolished the DNA damage-induced dynamic changes in O-GlcNAcylation (Figure 5D). Moreover, mutation of both Thr101 and Ser139 into Ala (2A) completely disrupted H2AX O-GlcNAcylation (Figure 5E). Taken together, these results suggest that O-GlcNAcylation on Ser139 is mainly induced by DNA damage, whereas O-GlcNAcylation on Thr101 is likely to be a basal level O-GlcNAcylation for other cellular functions. We also validated the results by performing the *in vitro* O-GlcNAcylation assays. Only the 2A mutant, but not the Thr101A mutant, failed to undergo OGT glycosylation (Figure 5F). Next, we validated the negative regulation of H2A Ser139 phosphorylation by O-GlcNAcylation in an *in vitro* assay. When the recombinant H2AX was glycosylated by OGT, the ATM-dependent H2AX phosphorylation at Ser139 was significantly suppressed (Figure 5G).

OGT negatively regulates the expansion of DNA damage-induced phosphorylation

In addition to evaluating H2AX, we also examined MDC1, the functional binding partner of γH2AX. Similar to

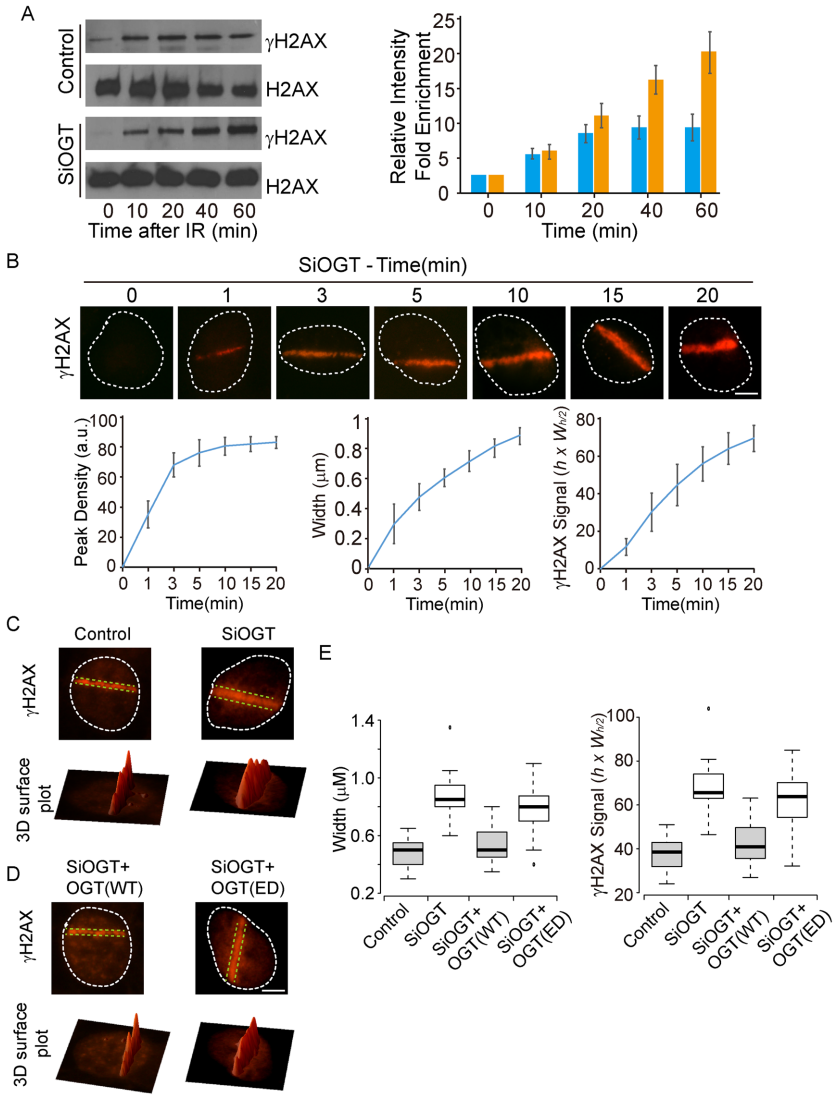

Figure 3. OGT negatively regulates γH2AX. (**A**) OGT suppresses DNA damage-induced H2AX phosphorylation. HeLa cells transfected with control or OGT siRNA were treated with 10 Gy of ionizing radiation (IR). The chromatin fractions were western blotted with the indicated antibodies. The relative band density of γH2AX was determined by Image J and plotted versus time. The lane labeled '0' represents un-irradiated cells and the γH2AX intensity of this lane was set as 1. (**B**) The kinetics of γH2AX recruitment in OGT knockdown cells (upper panel). The peak density, full width at half maximum, and overall γH2AX signal were plotted against time (lower panel). (**C** and **D**) OGT suppresses the expansion of γH2AX. HeLa cells transfected with control siRNA or OGT siRNA were subjected to laser micro-irradiation. γH2AX was evaluated using an anti-γH2AX antibody (C). OGT knockdown cells reconstituted with wild-type OGT or the enzyme-dead mutant (ED) were subjected to laser micro-irradiation. γH2AX was examined (D). 3D surface plots were generated by Image J. The IF intensity across the dash lines was analyzed by Image J software and plotted versus width (right panel). The dashed lines show the full width at half maximum of the laser strip in each cell. (**E**) The full width at half maximum and overall intensity of γH2AX signal were measured in each cell ($n = 10$) and box-plotted. For the box-plot: center lines show the medians; box limits indicate the 25th and 75th percentiles. $n = 10$. Scale bar: 5 μm. a.u.: arbitrary units.

H2AX, MDC1 was O-GlcNAcylated in response to DNA damage. Suppression of OGT by siRNA or by the OGT inhibitor ST045849 abolished the O-GlcNAcylation of MDC1 (Figure 6A and B). Moreover, O-GlcNAcylation of MDC1 suppressed PI3-like kinase-induced MDC1 phosphorylation, as detected by an anti-pSQTQ antibody, which specifically recognizes the substrates of ATM/ATR/DNA-PKcs (Figure 6A and B). These results suggest that O-GlcNAcylation also occurs in the functional partners of γH2AX, and may regulate overall signal transduction in response to DNA damage. We next examined the global phosphorylation level at the sites of DNA damage by IF, using an anti-pSQTQ antibody. Interestingly, the lack of OGT facilitated the expansion of these phosphorylation events, which is consistent our findings for γH2AX (Figure 6C). Furthermore, in contrast to wild-type OGT, the OGT (D6) mutant could not rescue the expansion of pSQTQ IF (Supplementary Figure S3C and E). These results suggest that O-GlcNAcylation acts as a negative regulator for DNA damage-induced phosphorylation events.

O-GlcNAcylation is a reversible PTM that can be erased by OGA (40,41). Similar to OGT, OGA was also re-

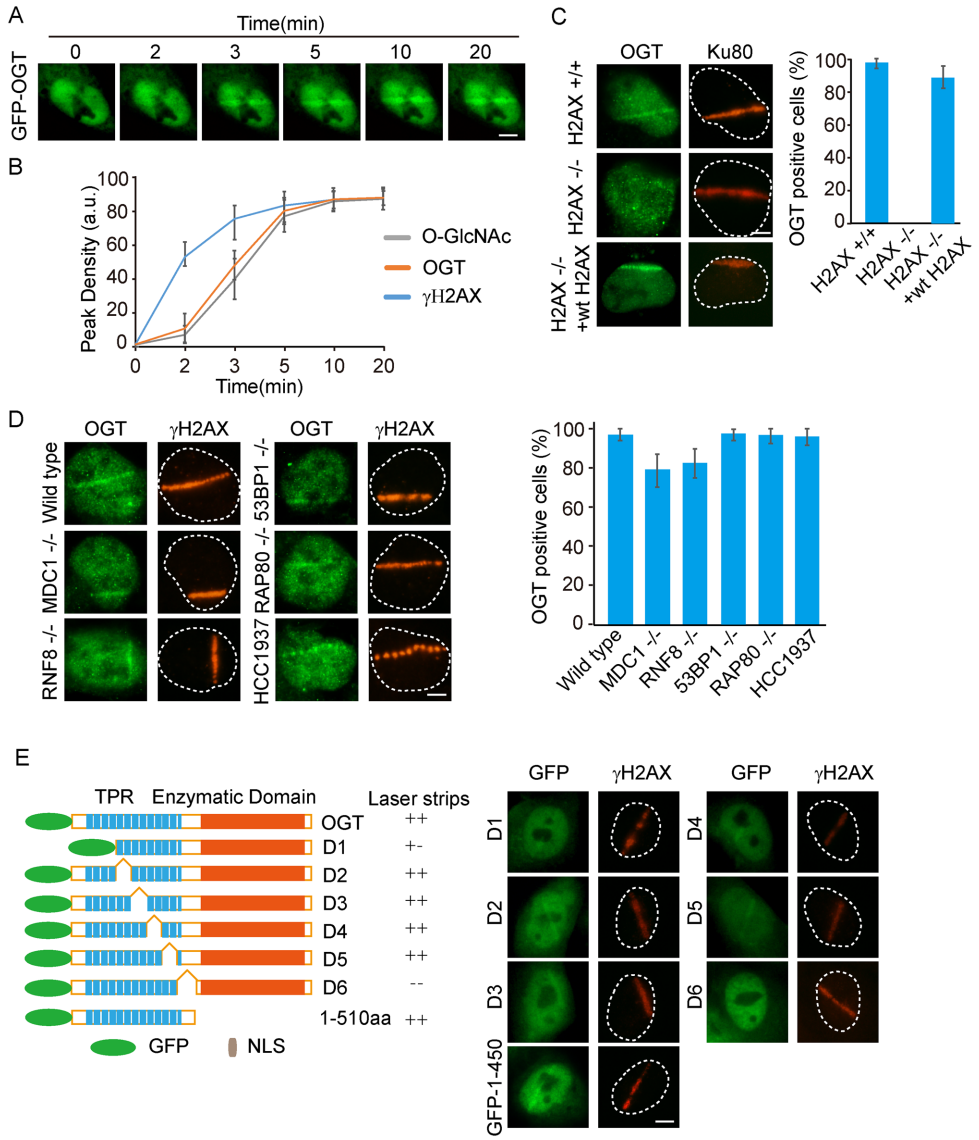

Figure 4. Dynamic localization of OGT following laser micro-irradiation. (**A**) The kinetics of OGT recruitment to the sites of DNA damage. HeLa cells expressing GFP-OGT were monitored after laser micro-irradiation. Scale bar: 5 μm. a.u.: arbitrary units. (**B**) Intensity of GFP-OGT at laser strips was quantified at the indicated time points and compared with O-GlcNAcylation and γH2AX. The peak IF density in the micro-irradiated areas was plotted versus time. (**C**) The recruitment of OGT relies on H2AX. H2AX +/+ and −/− MEFs, and H2AX −/− MEFs rescued with wt H2AX, were subjected to laser micro-irradiation. OGT and Ku80 were examined (left panel). The percentage of cells with OGT laser strips is shown (right panel). (**D**) Wild-type, MDC1 −/−, RNF8 −/−, RAP80 −/−, 53BP1 −/− MEFs and BRCA1-deficient HCC1937 cells were subjected to laser micro-irradiation. The recruitment of OGT was examined (left panel). The percentage of cells with OGT laser strips is shown (right panel). (**E**) The OGT linker region is required for the localization of OGT to the sites of DNA damage. Left panel: diagrams showing the OGT deletion mutants. Right panel: localization of OGT deletion mutants and γH2AX at the sites of DNA damage was assayed by IF.

cruited to the sites of DNA damage (Figure 6D). However, the kinetics of OGA recruitment were even slower than those of OGT. The recruitment of OGA provides another layer of regulation for DNA damage-induced signal transduction. Because suppression of OGA increases the O-GlcNAcylation level (42,43), we treated HeLa cells with the OGA inhibitor PUGNAc to suppress O-GlcNAcylation degradation (44) (Supplementary Figure S6) and then laser irradiated the cells. Interestingly, suppression of O-GlcNAcylation degradation delayed the expansion of DNA damage-induced phosphorylation (Figure 6E). Taken together, these results suggest that O-GlcNAcylation negatively regulates DNA damage response.

Loss of OGT prolongs G2/M checkpoint and decreases cell viability in response to DNA damage

We have shown that depletion of OGT disinhibits the phosphorylation of H2AX and MDC1. Because both γH2AX and MDC1 contribute to the activation of the DNA damage-induced G2/M checkpoint (19,20,45,46), we next tested the role of OGT in the G2/M checkpoint. In normal cells, IR treatment induces transient cell cycle arrest at

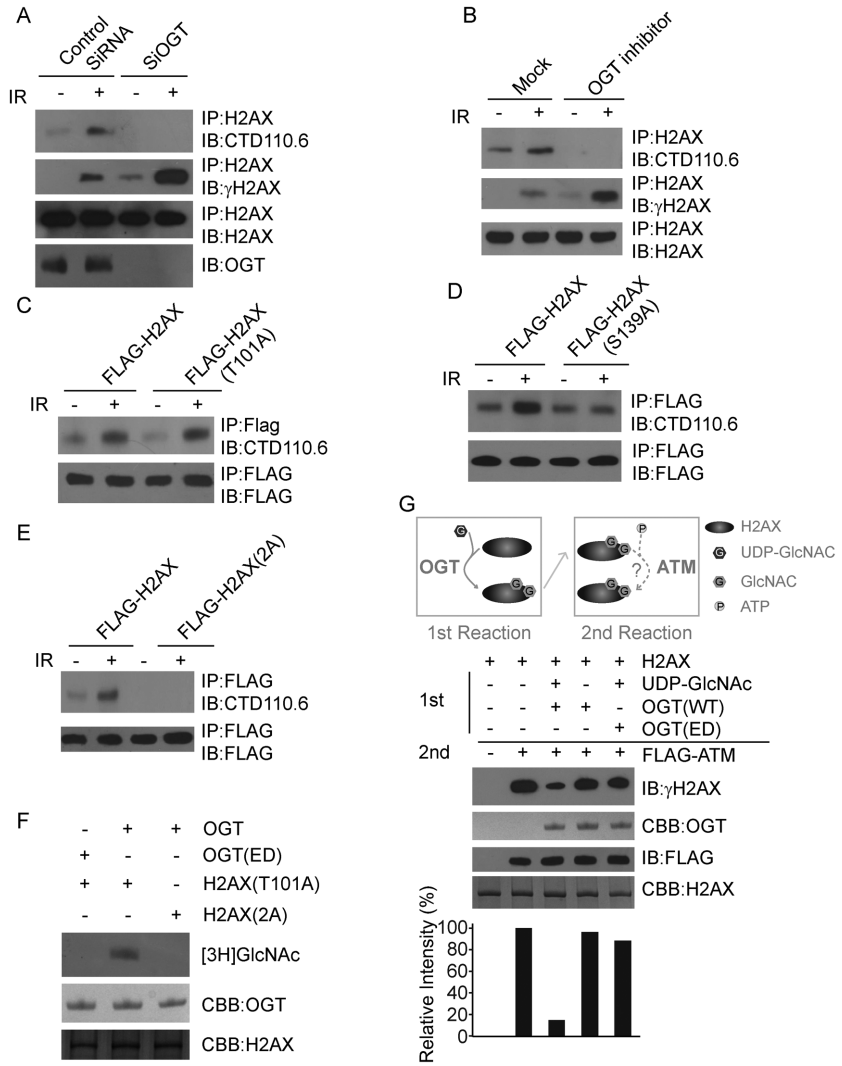

Figure 5. Ser 139 of H2AX is O-GlcNAcylated by OGT in response to DNA damage. (**A**) OGT is required for H2AX O-GlcNAcylation. HeLa cells transfected with control siRNA or OGT siRNA were treated with or without 10 Gy of IR. The cell lysates were analyzed by the indicated antibodies. (**B**) OGT inhibitor (ST045849) treatment suppresses H2AX O-GlcNAcylation. HeLa cells were treated with or without ST045849, followed by γ-irradiation. The cell lysates were analyzed with the indicated antibodies. (**C**) The T101A mutation does not affect DNA damage-induced H2AX O-GlcNAcylation. The 293T cells expressing FLAG-H2AX or the T101A mutant were treated with or without IR. The chromatin fractions were immunoprecipitated with an anti-FLAG antibody and western blotted with the indicated antibodies. (**D**) The S139A mutation abolishes the DNA damage-induced H2AX O-GlcNAcylation. The 293T cells expressing FLAG-H2AX or the S139A mutant were treated with or without IR. The chromatin fractions were immunoprecipitated with an anti-FLAG antibody and western blotted with indicated antibodies. (**E**) The 2A mutant is not glycosylated. The 293T cells expressing FLAG-H2AX or the 2A mutant were treated with or without IR. The chromatin fractions were immunoprecipitated with an anti-FLAG antibody and western blotted with the indicated antibodies (right panel). (**F**) H2AX is glycosylated by OGT *invitro*. Tritium-labeled GlcNAc was incorporated into the recombinant H2AX in the in vitro O-GlcNAcylation assays. Coomassie brilliant blue (CBB) staining was used as a loading control. (**G**) O-GlcNAcylation of H2AX blocks ATM-dependent H2AX phosphorylation. Recombinant H2AX was first glycosylated by OGT *invitro*, then subjected to the *invitro* phosphorylation assay with FLAG-ATM. The final products were western blotted using the indicated antibodies. The loading of recombinant H2AX is shown by CBB staining. The histogram shows the relative level of the γH2AX signal.

the G2/M transition, which allows cells to repair DNA lesions before entering mitosis. This transient G2/M checkpoint is mediated by a γH2AX-dependent pathway (47), and only lasts for 1–2 h. Unrepaired lesions prolong the G2/M checkpoint, activate apoptotic pathways and induce cell lethality, which prevents cells with lesions from entering mitosis.

To study the role of OGT in this process, we examined Chk1 activation, because Chk1 is a downstream effector of the γH2AX-dependent pathway for G2/M checkpoint activation (48–51). Interestingly, we found that Ser345 phosphorylation of Chk1, a surrogate marker of Chk1 activation, persisted for 5 h after IR treatment in OGT-depleted cells (Figure 7A), unlike our results in control cells. Consistently, we found that OGT depletion constitutively arrested cells at the G2/M transition, as indicated by histone H3 pS10 positive staining. However, in the control cells, mitosis fully recovered within 4 h after IR treatment (Figure 7C). Moreover, we treated OGT-depleted cells with the ATM inhibitor KU-55933 to shut down ATM activation

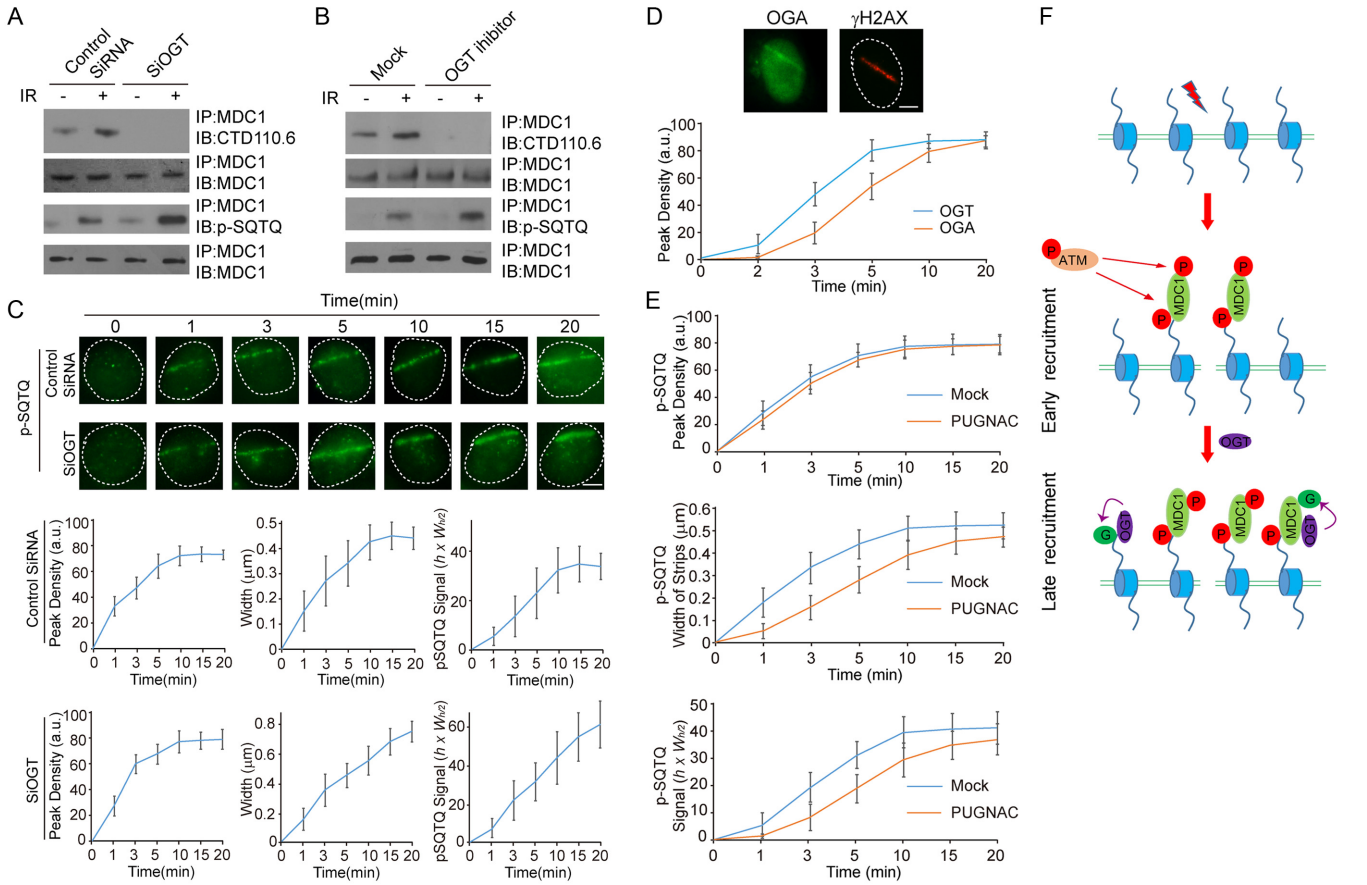

Figure 6. OGT regulates other DNA damage-induced phosphorylation events. (**A**) MDC1 is O-GlcNAcylated by OGT in response to DNA damage. HeLa cells were transfected with control or OGT siRNA. The cells were treated with 10 Gy of IR. The lysates were immunoprecipitated by an anti-MDC1 antibody and analyzed by western blotting with indicated antibodies. (**B**) An OGT inhibitor (ST045849) suppresses DNA damage-induced MDC1 O-GlcNAcylation. ST045849-treated HeLa cells were immunoprecipitated by anti-MDC1 antibody and analyzed by western blotting with indicated antibodies. (**C**) OGT negatively regulates the expansion of ATM-dependent phosphorylation events at the sites of DNA damage. OGT knockdown cells were subjected to laser micro-irradiation and ATM substrates was assayed with an anti-pSQTQ antibody. (**D**) OGA is recruited to the sites of DNA damage. HeLa cells were subjected to laser micro-irradiation. Kinetics of the recruitment of OGA was examined (lower panel). (**E**) An OGA inhibitor (PUGNAc) suppresses the expansion of pSQTQ. HeLa cells were treated with PUGNAc and followed by laser micro-irradiation. The peak density, full width at half maximum and overall pSQTQ signal were quantified at indicated time points. (**F**) Model of DNA damage-induced O-GlcNAcylation.

1 h after IR treatment (Figure 7B). The ATM inhibitor treatment could partially rescue the G2/M transition arrest in the OGT-depleted cells (Figure 7C and D). Finally, the G2/M transition arrest in the OGT-depleted cells could be rescued by wild-type OGT but not by the enzyme-dead mutant of OGT (Figure 7D). These results suggested that O-GlcNAcylation suppresses the γH2AX-dependent pathway for limiting the G2/M checkpoint. To exclude the possibility that the prolonged G2/M checkpoint is because of unrepaired DNA lesions, we performed comet assays and found that DSB repair is unaffected by OGT depletion (Supplementary Figure S7).

Because prolongation of the G2/M checkpoint activates apoptosis, we next studied the role of OGT in cell viability after DNA damage. Compared to the mock treated cells, the OGT-depleted cells were hypersensitive to low doses of IR (Figure 7E). Again, only wild-type OGT, but not the enzyme-dead mutant, could rescue the cell lethality, suggesting that O-GlcNAcylation plays an important role in limiting the DNA damage response and promoting cell viability.

DISCUSSION

In this study, we have demonstrated that OGT-dependent O-GlcNAcylation is enriched at the sites of DNA damage and negatively regulates DNA damage response. Loss of OGT causes un-controlled expansion of the DNA damage response, due to loss of O-GlcNAcylation on H2AX and other factors. This result suggests that OGT-induced O-GlcNAcylation plays a critical role in the normal cellular response to DNA damage.

Similar to many other PTMs, O-GlcNAcylation is induced by DSBs, DNA crosslinking damage and DNA alkylation damage. With IR treatment, we found that both H2AX and MDC1 were O-GlcNAcylated by OGT. We have mapped Ser139 as the major DNA damage-induced O-GlcNAcylation site in H2AX. Because Ser139 of H2AX is also phosphorylated by ATM/ATR/DNA-PK (13,15–17), O-GlcNAcylation competes with phosphorylation on

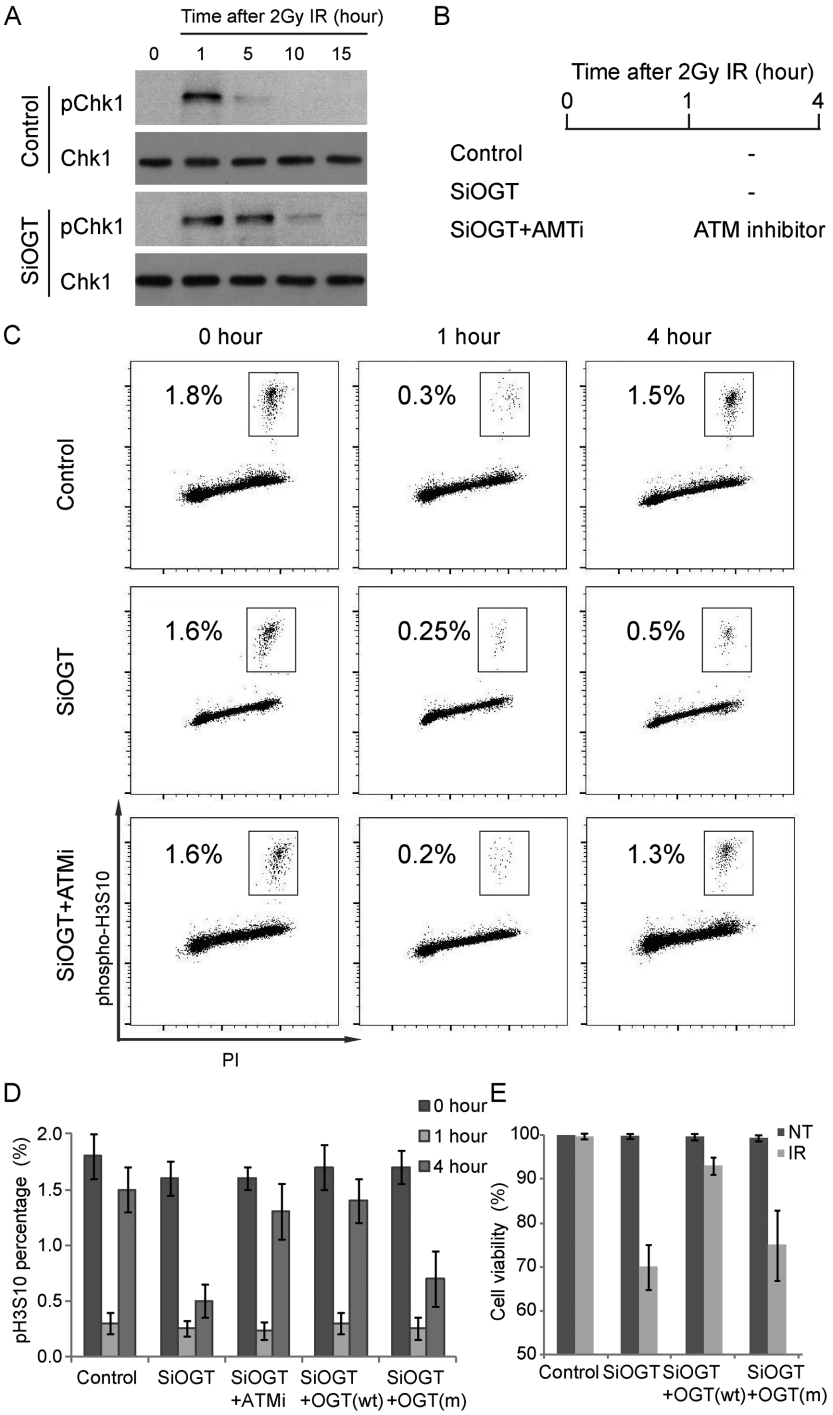

Figure 7. Depletion of OGT prolongs the G2/M checkpoint and reduces cell viability following DNA damage. (**A**) Control or OGT-depleted HeLa cells were treated with 5 Gy of IR and released. The cells were collected at the indicated time point and the cell lysates were western blotted with the indicated antibodies. (**B** and **C**) Control or OGT-depleted HeLa cells were treated with 2 Gy of IR and released. After 1 h, an ATM inhibitor (KU-55933) was added to block G2/M checkpoint activation (B). The cells were collected at the indicated time point, stained with anti-phospho-H3 S10 antibody and analyzed by flow cytometry (C). (**D**) The percentage of phosphorylation H3 S10-positive cells in the indicated conditions was shown. The data are presented as mean ± SD. (**E**) HeLa cells expressing control siRNA (Control), OGT siRNA (siOGT) or a combination of OGT siRNA and siRNA-resistant wild-type OGT (siOGT + OGT (wt)) or enzyme-dead OGT (siOGT + OGT (m)), were treated with 2 Gy of IR. Forty-eight hours later, the viability of the treated cells was determined using the CellTiter-Blue reagent.

H2AX. Moreover, O-GlcNAcylation of H2AX is induced by γH2AX and acts as a negative feedback regulator to limit the expansion of γH2AX at the site of DNA damage (Figure 6F). Consistently, the enrichment of O-GlcNAcylation at the sites of DNA damage occurs when the expansion of γH2AX reaches a steady state. Thus, our study reveals another layer of γH2AX regulation at the site of DNA damage.

Interestingly, O-GlcNAcylation of H2AX does not affect the peak level of γH2AX, but instead limits the expansion of γH2AX. It is likely that the position of the peak γH2AX intensity is located close to the sites of DNA damage. Most H2AX at the sites of DNA damage has already been phosphorylated by ATM/ATR/DNA-PK within a very short period. Once H2AX is phosphorylated, it recruits OGT to O-GlcNAcylate the adjacent H2AX regions and arrests the expansion of the γH2AX signal. It is also intriguing to note that both the TPR domain and the catalytic domain mediate OGT recruitment to the sites of DNA damage. Because the TPR domain and the catalytic domain function together to catalyze substrate O-GlcNAcylation (27), substrate recognition could be the molecular mechanism by which OGT is recruited to the sites of DNA damage. However, interaction between enzymes and substrates is very transient; otherwise the enzyme will be trapped by the substrate. Therefore, we did not observe a stable interaction between OGT and H2AX. This process is very similar to H2AX phosphorylation. In response to DNA damage, ATM is recruited to the sites of DNA damage and phosphorylates H2AX via a very transient interaction (19).

In addition to H2AX, we also found that MDC1 was O-GlcNAcylated in response to DNA damage. Similar to O-GlcNAcylation of H2AX, O-GlcNAcylation of MDC1 suppresses DNA damage-induced phosphorylation of MDC1. Because MDC1 is phosphorylated by ATM at multiple sites (52,53), it is likely that OGT also induces O-GlcNAcylation at multiple sites to suppress ATM-dependent phosphorylation. Similar results are also obtained by observing the general ATM substrate using an anti-pSQTQ antibody, suggesting that O-GlcNAcylation is likely to form a negative feedback loop to suppress ATM-dependent signaling.

Moreover, due to our research focus, we did not test other types of DNA damage. However, it is possible that other types of DNA damage, such as DNA single-strand breaks, may also induce O-GlcNAcylation, albeit on different substrates.

We also found that OGT depletion reduces cell viability in response to DNA damage. Interestingly, OGT depletion does not impair the DNA damage repair process. However, we found that prolongation of the G2/M checkpoint delayed cell cycle recovery from IR treatment. It is likely that uncontrolled phosphorylation of H2AX and MDC1 prolongs G2/M arrest by constitutively activating Chk1. This prolonged G2/M checkpoint eventually induces apoptosis (54–58). Therefore, OGT is likely to act as a negative regulator to restrain the local DNA damage response and help cells recover from DNA repair. Of note, the peak level of H2AX phosphorylation does not change in the OGT-deficient cells. Instead, the expansion of H2AX phosphorylation is deregulated in OGT-deficient cells. Therefore, it is likely that the precisely regulated γH2AX expansion plays a key role in the G2/M checkpoint.

To date, the DNA damage-induced signals have been well studied. However, these signals are mainly restricted to the sites of DNA damage, so that local DNA damage would not affect other cellular events, such as transcription, at the undamaged regions. Our study shows that OGT is one of the important negative regulators that limit the expansion of DNA damage-induced signaling. Besides O-GlcNAcylation, other mechanisms also act as negative feedback regulators to suppress DNA damage-induced signaling (59).

SUPPLEMENTARY DATA

Supplementary Data are available at NAR Online.

FUNDING

National Institutes of Health [CA132755, CA130899 to X.Y.]; Department of Defense, Era of Hope Scholar Award (to X.Y.); Leukemia and Lymphoma Society Scholar Award (to X.Y.). Funding from open access charge: National Institute of Health.
Conflict of interest statement. None declared.

REFERENCES

1. Fernandez-Capetillo,O., Celeste,A. and Nussenzweig,A. (2003) Focusing on foci: H2AX and the recruitment of DNA-damage response factors. *Cell Cycle*, **2**, 426–427.
2. Petrini,J.H. and Stracker,T.H. (2003) The cellular response to DNA double-strand breaks: defining the sensors and mediators. *Trends Cell Biol.*, **13**, 458–462.
3. Paull,T.T., Rogakou,E.P., Yamazaki,V., Kirchgessner,C.U., Gellert,M. and Bonner,W.M. (2000) A critical role for histone H2AX in recruitment of repair factors to nuclear foci after DNA damage. *Curr. Biol.*, **10**, 886–895.
4. Falck,J., Coates,J. and Jackson,S.P. (2005) Conserved modes of recruitment of ATM, ATR and DNA-PKcs to sites of DNA damage. *Nature*, **434**, 605–611.
5. Polo,S.E. and Jackson,S.P. (2011) Dynamics of DNA damage response proteins at DNA breaks: a focus on protein modifications. *Genes Dev.*, **25**, 409–433.
6. Ismail,I.H. and Hendzel,M.J. (2008) The gamma-H2A.X: is it just a surrogate marker of double-strand breaks or much more? *Environ. Mol. Mutagen.*, **49**, 73–82.
7. Jackson,S.P. and Durocher,D. (2013) Regulation of DNA damage responses by ubiquitin and SUMO. *Mol. Cell*, **49**, 795–807.
8. Ma,T., Chen,Y., Zhang,F., Yang,C.Y., Wang,S. and Yu,X. (2013) RNF111-dependent neddylation activates DNA damage-induced ubiquitination. *Mol. Cell*, **49**, 897–907.
9. Rogakou,E.P., Pilch,D.R., Orr,A.H., Ivanova,V.S. and Bonner,W.M. (1998) DNA double-stranded breaks induce histone H2AX phosphorylation on serine 139. *J. Biol. Chem.*, **273**, 5858–5868.
10. Rogakou,E.P., Boon,C., Redon,C. and Bonner,W.M. (1999) Megabase chromatin domains involved in DNA double-strand breaks in vivo. *J. Cell Biol.*, **146**, 905–916.
11. Cortez,D., Wang,Y., Qin,J. and Elledge,S.J. (1999) Requirement of ATM-dependent phosphorylation of brca1 in the DNA damage response to double-strand breaks. *Science*, **286**, 1162–1166.
12. Lim,D.S., Kim,S.T., Xu,B., Maser,R.S., Lin,J., Petrini,J.H. and Kastan,M.B. (2000) ATM phosphorylates p95/nbs1 in an S-phase checkpoint pathway. *Nature*, **404**, 613–617.
13. Burma,S., Chen,B.P., Murphy,M., Kurimasa,A. and Chen,D.J. (2001) ATM phosphorylates histone H2AX in response to DNA double-strand breaks. *J. Biol. Chem.*, **276**, 42462–42467.

14. Bakkenist,C.J. and Kastan,M.B. (2003) DNA damage activates ATM through intermolecular autophosphorylation and dimer dissociation. *Nature*, **421**, 499–506.
15. Ward,I.M. and Chen,J. (2001) Histone H2AX is phosphorylated in an ATR-dependent manner in response to replicational stress. *J. Biol. Chem.*, **276**, 47759–47762.
16. Stiff,T., O'Driscoll,M., Rief,N., Iwabuchi,K., Lobrich,M. and Jeggo,P.A. (2004) ATM and DNA-PK function redundantly to phosphorylate H2AX after exposure to ionizing radiation. *Cancer Res.*, **64**, 2390–2396.
17. Reitsema,T., Klokov,D., Banath,J.P. and Olive,P.L. (2005) DNA-PK is responsible for enhanced phosphorylation of histone H2AX under hypertonic conditions. *DNA Repair*, **4**, 1172–1181.
18. Mukherjee,B., Kessinger,C., Kobayashi,J., Chen,B.P., Chen,D.J., Chatterjee,A. and Burma,S. (2006) DNA-PK phosphorylates histone H2AX during apoptotic DNA fragmentation in mammalian cells. *DNA Repair*, **5**, 575–590.
19. Stucki,M., Clapperton,J.A., Mohammad,D., Yaffe,M.B., Smerdon,S.J. and Jackson,S.P. (2005) MDC1 directly binds phosphorylated histone H2AX to regulate cellular responses to DNA double-strand breaks. *Cell*, **123**, 1213–1226.
20. Lou,Z., Minter-Dykhouse,K., Franco,S., Gostissa,M., Rivera,M.A., Celeste,A., Manis,J.P., van Deursen,J., Nussenzweig,A., Paull,T.T. *et al.* (2006) MDC1 maintains genomic stability by participating in the amplification of ATM-dependent DNA damage signals. *Mol. Cell*, **21**, 187–200.
21. Huen,M.S., Grant,R., Manke,I., Minn,K., Yu,X., Yaffe,M.B. and Chen,J. (2007) RNF8 transduces the DNA-damage signal via histone ubiquitylation and checkpoint protein assembly. *Cell*, **131**, 901–914.
22. Mailand,N., Bekker-Jensen,S., Faustrup,H., Melander,F., Bartek,J., Lukas,C. and Lukas,J. (2007) RNF8 ubiquitylates histones at DNA double-strand breaks and promotes assembly of repair proteins. *Cell*, **131**, 887–900.
23. Kim,J.S., Krasieva,T.B., Kurumizaka,H., Chen,D.J., Taylor,A.M. and Yokomori,K. (2005) Independent and sequential recruitment of NHEJ and HR factors to DNA damage sites in mammalian cells. *J. Cell Biol.*, **170**, 341–347.
24. Haltiwanger,R.S., Blomberg,M.A. and Hart,G.W. (1992) Glycosylation of nuclear and cytoplasmic proteins. Purification and characterization of a uridine diphospho-N-acetylglucosamine:polypeptide beta-N-acetylglucosaminyltransferase. *J. Biol. Chem.*, **267**, 9005–9013.
25. Kreppel,L.K., Blomberg,M.A. and Hart,G.W. (1997) Dynamic glycosylation of nuclear and cytosolic proteins. Cloning and characterization of a unique O-GlcNAc transferase with multiple tetratricopeptide repeats. *J. Biol. Chem.*, **272**, 9308–9315.
26. Wells,L., Vosseller,K. and Hart,G.W. (2001) Glycosylation of nucleocytoplasmic proteins: signal transduction and O-GlcNAc. *Science*, **291**, 2376–2378.
27. Lazarus,M.B., Nam,Y., Jiang,J., Sliz,P. and Walker,S. (2011) Structure of human O-GlcNAc transferase and its complex with a peptide substrate. *Nature*, **469**, 564–567.
28. Chou,T.Y., Hart,G.W. and Dang,C.V. (1995) c-Myc is glycosylated at threonine 58, a known phosphorylation site and a mutational hot spot in lymphomas. *J. Biol. Chem.*, **270**, 18961–18965.
29. Comer,F.I. and Hart,G.W. (2001) Reciprocity between O-GlcNAc and O-phosphate on the carboxyl terminal domain of RNA polymerase II. *Biochemistry*, **40**, 7845–7852.
30. Ranuncolo,S.M., Ghosh,S., Hanover,J.A., Hart,G.W. and Lewis,B.A. (2012) Evidence of the involvement of O-GlcNAc-modified human RNA polymerase II CTD in transcription in vitro and in vivo. *J. Biol. Chem.*, **287**, 23549–23561.
31. Hart,G.W., Slawson,C., Ramirez-Correa,G. and Lagerlof,O. (2011) Cross talk between O-GlcNAcylation and phosphorylation: roles in signaling, transcription, and chronic disease. *Annu. Rev. Biochem.*, **80**, 825–858.
32. Zachara,N.E., Molina,H., Wong,K.Y., Pandey,A. and Hart,G.W. (2011) The dynamic stress-induced "O-GlcNAc-ome" highlights functions for O-GlcNAc in regulating DNA damage/repair and other cellular pathways. *Amino Acids*, **40**, 793–808.
33. Hahne,H., Sobotzki,N., Nyberg,T., Helm,D., Borodkin,V.S., van Aalten,D.M., Agnew,B. and Kuster,B. (2013) Proteome wide purification and identification of O-GlcNAc-modified proteins using click chemistry and mass spectrometry. *J. Proteome Res.*, **12**, 927–936.
34. Zhong,J., Martinez,M., Sengupta,S., Lee,A., Wu,X., Chaerkady,R., Chatterjee,A., O'Meally,R.N., Cole,R.N., Pandey,A. *et al.* (2015) Quantitative phosphoproteomics reveals crosstalk between phosphorylation and O-GlcNAc in the DNA damage response pathway. *Proteomics*, **15**, 591–607.
35. Singh,J.P., Zhang,K., Wu,J. and Yang,X. (2015) O-GlcNAc signaling in cancer metabolism and epigenetics. *Cancer Lett.*, **356**, 244–250.
36. Wang,Z., Gucek,M. and Hart,G.W. (2008) Cross-talk between GlcNAcylation and phosphorylation: site-specific phosphorylation dynamics in response to globally elevated O-GlcNAc. *Proc. Natl. Acad. Sci. U.S.A.*, **105**, 13793–13798.
37. Chen,Q., Chen,Y., Bian,C., Fujiki,R. and Yu,X. (2013) TET2 promotes histone O-GlcNAcylation during gene transcription. *Nature*, **493**, 561–564.
38. Li,M. and Yu,X. (2013) Function of BRCA1 in the DNA damage response is mediated by ADP-ribosylation. *Cancer Cell*, **23**, 693–704.
39. Sakabe,K., Wang,Z. and Hart,G.W. (2010) Beta-N-acetylglucosamine (O-GlcNAc) is part of the histone code. *Proc. Natl. Acad. Sci. U.S.A.*, **107**, 19915–19920.
40. Dong,D.L. and Hart,G.W. (1994) Purification and characterization of an O-GlcNAc selective N-acetyl-beta-D-glucosaminidase from rat spleen cytosol. *J. Biol. Chem.*, **269**, 19321–19330.
41. Wells,L., Gao,Y., Mahoney,J.A., Vosseller,K., Chen,C., Rosen,A. and Hart,G.W. (2002) Dynamic O-glycosylation of nuclear and cytosolic proteins: further characterization of the nucleocytoplasmic beta-N-acetylglucosaminidase, O-GlcNAcase. *J. Biol. Chem.*, **277**, 1755–1761.
42. Gloster,T.M. and Vocadlo,D.J. (2010) Mechanism, Structure, and Inhibition of O-GlcNAc Processing Enzymes. *Curr. Signal Transduct. Ther.*, **5**, 74–91.
43. Macauley,M.S. and Vocadlo,D.J. (2010) Increasing O-GlcNAc levels: an overview of small-molecule inhibitors of O-GlcNAcase. *Biochim. Biophys. Acta*, **1800**, 107–121.
44. Haltiwanger,R.S., Grove,K. and Philipsberg,G.A. (1998) Modulation of O-linked N-acetylglucosamine levels on nuclear and cytoplasmic proteins in vivo using the peptide O-GlcNAc-beta-N-acetylglucosaminidase inhibitor O-(2-acetamido-2-deoxy-D-glucopyranosylidene)amino-N-phenylcarbamate. *J. Biol. Chem.*, **273**, 3611–3617.
45. Kobayashi,J., Antoccia,A., Tauchi,H., Matsuura,S. and Komatsu,K. (2004) NBS1 and its functional role in the DNA damage response. *DNA Repair*, **3**, 855–861.
46. Bekker-Jensen,S., Lukas,C., Kitagawa,R., Melander,F., Kastan,M.B., Bartek,J. and Lukas,J. (2006) Spatial organization of the mammalian genome surveillance machinery in response to DNA strand breaks. *J. Cell Biol.*, **173**, 195–206.
47. Fernandez-Capetillo,O., Chen,H.T., Celeste,A., Ward,I., Romanienko,P.J., Morales,J.C., Naka,K., Xia,Z., Camerini-Otero,R.D., Motoyama,N. *et al.* (2002) DNA damage-induced G2-M checkpoint activation by histone H2AX and 53BP1. *Nat. Cell Biol.*, **4**, 993–997.
48. Lou,Z., Minter-Dykhouse,K., Wu,X. and Chen,J. (2003) MDC1 is coupled to activated CHK2 in mammalian DNA damage response pathways. *Nature*, **421**, 957–961.
49. Kim,H., Chen,J. and Yu,X. (2007) Ubiquitin-binding protein RAP80 mediates BRCA1-dependent DNA damage response. *Science*, **316**, 1202–1205.
50. Stewart,G.S., Wang,B., Bignell,C.R., Taylor,A.M. and Elledge,S.J. (2003) MDC1 is a mediator of the mammalian DNA damage checkpoint. *Nature*, **421**, 961–966.
51. Yarden,R.I., Pardo-Reoyo,S., Sgagias,M., Cowan,K.H. and Brody,L.C. (2002) BRCA1 regulates the G2/M checkpoint by activating Chk1 kinase upon DNA damage. *Nat. Genet.*, **30**, 285–289.
52. Stucki,M. and Jackson,S.P. (2004) MDC1/NFBD1: a key regulator of the DNA damage response in higher eukaryotes. *DNA Repair*, **3**, 953–957.
53. Deplus,R., Delatte,B., Schwinn,M.K., Defrance,M., Mendez,J., Murphy,N., Dawson,M.A., Volkmar,M., Putmans,P., Calonne,E. *et al.* (2013) TET2 and TET3 regulate GlcNAcylation and H3K4 methylation through OGT and SET1/COMPASS. *EMBO J.*, **32**, 645–655.

54. Hirao,A., Cheung,A., Duncan,G., Girard,P.M., Elia,A.J., Wakeham,A., Okada,H., Sarkissian,T., Wong,J.A., Sakai,T. *et al.* (2002) Chk2 is a tumor suppressor that regulates apoptosis in both an ataxia telangiectasia mutated (ATM)-dependent and an ATM-independent manner. *Mol. Cell. Biol.*, **22**, 6521–6532.
55. Jack,M.T., Woo,R.A., Hirao,A., Cheung,A., Mak,T.W. and Lee,P.W. (2002) Chk2 is dispensable for p53-mediated G1 arrest but is required for a latent p53-mediated apoptotic response. *Proc. Natl. Acad. Sci. U.S.A.*, **99**, 9825–9829.
56. Bartek,J. and Lukas,J. (2003) Chk1 and Chk2 kinases in checkpoint control and cancer. *Cancer Cell*, **3**, 421–429.
57. Zhou,B.B. and Elledge,S.J. (2000) The DNA damage response: putting checkpoints in perspective. *Nature*, **408**, 433–439.
58. Sturgeon,C.M., Knight,Z.A., Shokat,K.M. and Roberge,M. (2006) Effect of combined DNA repair inhibition and G2 checkpoint inhibition on cell cycle progression after DNA damage. *Mol. Cancer Ther.*, **5**, 885–892.
59. Altmeyer,M., Toledo,L., Gudjonsson,T., Grofte,M., Rask,M.B., Lukas,C., Akimov,V., Blagoev,B., Bartek,J. and Lukas,J. (2013) The chromatin scaffold protein SAFB1 renders chromatin permissive for DNA damage signaling. *Mol. Cell*, **52**, 206–220.